



UNIVERSITY OF LEEDS

This is a repository copy of *Structures and orientation-dependent interaction forces of titania nanowires using molecular dynamics simulations*.

White Rose Research Online URL for this paper:  
<http://eprints.whiterose.ac.uk/117681/>

Version: Accepted Version

---

**Article:**

Okeke, G, Antony, SJ [orcid.org/0000-0003-1761-6306](https://orcid.org/0000-0003-1761-6306), Hammond, RB et al. (1 more author) (2017) Structures and orientation-dependent interaction forces of titania nanowires using molecular dynamics simulations. *Journal of Nanoparticle Research*, 19 (7). 237. ISSN 1388-0764

<https://doi.org/10.1007/s11051-017-3930-7>

---

© 2017, Springer Science+Business Media B.V. This is an author produced version of a paper published in *Journal of Nanoparticle Research*. The final publication is available at Springer via <https://doi.org/10.1007/s11051-017-3930-7>. Uploaded in accordance with the publisher's self-archiving policy.

**Reuse**

Items deposited in White Rose Research Online are protected by copyright, with all rights reserved unless indicated otherwise. They may be downloaded and/or printed for private study, or other acts as permitted by national copyright laws. The publisher or other rights holders may allow further reproduction and re-use of the full text version. This is indicated by the licence information on the White Rose Research Online record for the item.

**Takedown**

If you consider content in White Rose Research Online to be in breach of UK law, please notify us by emailing [eprints@whiterose.ac.uk](mailto:eprints@whiterose.ac.uk) including the URL of the record and the reason for the withdrawal request.



[eprints@whiterose.ac.uk](mailto:eprints@whiterose.ac.uk)  
<https://eprints.whiterose.ac.uk/>

Credit: Journal of Nanoparticle Research (Accepted version)

## **Structures and orientation-dependent interaction forces of titania nanowires using molecular dynamics simulations**

*George Okeke, S. Joseph Antony\*, Robert B. Hammond and Kamran Ahmed*

School of Chemical and Process Engineering, University of Leeds, Leeds LS2 9JT, UK

\*Corresponding author: [S.J.Antony@leeds.ac.uk](mailto:S.J.Antony@leeds.ac.uk)

### **Abstract**

Engineering nano wires to develop new products and processes is highly topical due to their ability to provide highly enhanced physical, chemical, mechanical, thermal and electrical properties. In this work, using molecular dynamics simulations, we report fundamental information, about the structural and thermodynamic properties of individual anatase titania (TiO<sub>2</sub>) nanowires with cross-sectional diameters between 2 and 6 nm, and aspect ratio (Length: Diameter) of 6:1 at temperatures ranging from 300 to 3000 K. Estimates of the melting-transition temperature of the nanowires are between 2000 and 2500 K. The melting transition temperature predicted from the radial distribution functions (RDFs) shows strong agreement with those predicted from the total energy profiles. Overall, the transition temperature is in reasonable agreement with melting points predicted from experiments and simulations reported in the literature for spherical nanoparticles of similar sizes. Hence, the melting-transition temperature of TiO<sub>2</sub> nanowires modelled here can be considered as shape independent. Furthermore, for the first time based on MD simulations, interaction forces between two nanowires are reported at ambient temperature (300 K) for different orientations: parallel, perpendicular, and end-to-end. It is observed that end-to-end orientations manifested the

strongest attraction forces, while the parallel and perpendicular orientations, displayed weaker attractions. The results reported here could form a foundation in future multiscale modelling studies of the structured titania nanowire assemblies, depending on the inter-wire interaction forces.

**Keywords:** MD simulations, RDF, potential energy, interaction forces, anatase, titania

## 1 Introduction

Recently there has been a growing interest in understanding the properties of nanoparticles and their applications as they possess superior physical, chemical, thermal and electrical properties. These properties make nanoparticles highly desirable in a wide range of industries and application areas including photonics (Gorkhover et al., 2016), chemical sensors (Zheng et al., 2000), catalysis (Chaudhari et al., 2006; Haverkamp, 2010; Soo-Jin Park, 2010) and electronics (Karmakar et al., 2011). The use of nanoparticles, in the form of metallic oxides, in base fluids for engineering applications is fast evolving. It has been observed through experiments (Ding et al., 2010; Garg et al., 2009) and numerical modelling (Okeke et al., 2011), that the suspension of nanoparticles in conventional heat transfer fluids such as water and ethylene glycol enhances the heat transfer properties of the fluids. Nanoparticles such as nanowires are also a novel class of functional materials with significant potential to be developed into innovative, smart devices and systems (Francioso et al., 2008). The shape of these particles provides them with enhanced optical and electrical properties, making them useful in a wide variety of applications. For example, they can be synthesized in controlled conditions as semiconductors with enhanced electrical transport properties (Chen and Mao, 2006). They are also used in innovative, dye-sensitized solar cells (DSSC) with enhanced performance of electron movement, offering low-cost materials (Mohd Azlishah et al., 2014). Nanowires also have enhanced photo-electrochemical properties as they can decouple the directions of light absorption and charge

carrier collections (Hwang et al., 2012). Nanoparticles are also applied in the area of medicine for drug targeting and delivery, in vitro and in vivo diagnostics, reduced toxicity, as well as production of enhanced biocompatible materials (Duncan, 2003; Ferrari, 2005). They are highly desirable in this area due to their large surface area to mass ratio and quantum properties which give them the ability to adsorb and transport other compounds such as drugs, probes and proteins (De Jong and Borm, 2008). They are currently being applied in the treatment of cancer using injectable drug delivery technologies to aid in targeting tumour cells (Ferrari, 2005). Most recently, a new self-reporting nanomedicine is developed to deliver chemotherapy or immunotherapy as well as report the effectiveness of the therapy in real-time (Kulkarni et al., 2016). Such applications could depend on fundamental level information about nanoparticles such as their structural orientations under different thermal conditions and the interaction forces between contiguous nano wires.

In the current work, molecular dynamics simulations are carried out for anatase titania nanowires of different cross-sectional diameters over a range of temperatures. The focus is on understanding their structural properties and inter-wire force-separation relations. It is anticipated that these properties will play an important role in application areas such as energy generation and storage and targeted drug delivery (Pritesh et al., 2012; De Jong and Borm, 2008). Titania has been investigated widely due to its many desirable properties, including low cost (Lin et al., 2012), ease of production (Mahshid et al., 2007) and recyclability (Abdullah et al., 2016). It exists in three crystalline forms namely rutile, anatase and brookite, with rutile and anatase, being the most important forms. Using molecular dynamics simulations, studies on  $\text{TiO}_2$  nanospheres have been carried out previously, to understand their thermal characteristics such as melting transition temperature, as well as structural properties (Okeke et al., 2016). In this, the melting point of the nanospheres was evaluated from the variation in the potential energy of the system as a function of temperature. Also, the radial distribution

functions (RDF's) of the nanoparticles were linked to the variation of potential energy of the system with temperature. It was observed that changes in the gradient of a plot of potential energy versus temperature associated with the melting transition occurred at temperatures similar to those associated with the broadening of peaks in the RDFs (Okeke et al., 2016). Here, using a similar approach, we investigate these properties for TiO<sub>2</sub> nanowires with cross-sectional diameters ranging from 2 to 6 nm at temperatures from 300 to 3000 K in a vacuum. Furthermore, we investigate the interaction force between two nanowires with respect to separation distance and orientation using molecular dynamics simulations. These forces are known to influence the inter-particle interactions and are useful in understanding the processing behaviour for particle assemblies such as aggregation, packing, flowability, adsorption, and stability (Zeng et al., 2010; Boal et al., 2000; Xu et al., 2006; Dong et al., 2006). The ordering and assembly of particles into defined structures can be controlled by exploiting the inherent inter-particle interactions. For example, by heating and applying surface pressure, nanorods can be engineered into nanowires as a result of a controlled, irreversible coalescence of the rods at the air-water interface (Min et al., 2008; Pradhan and Efrima, 2004; Acharya and Efrima, 2005). Understanding interaction forces between nanoparticles at different mutual-orientations will provide more insight into their assembly into various microstructures for a wide range of functional applications. The current work illustrates an approach for predicting such forces as a function of particle orientation, which has never been exploited before, to the best of our knowledge, especially for nanowires.

## **2 Simulation details**

### **2.1 Creation of nanoparticles**

Three dimensional anatase TiO<sub>2</sub> nanowires (nano rods of circular cross-section) were created using the BIOVIA Materials Studio 7.0 modelling package (*Materials Studio suite of*

*crystallographic programs*). This package is used to study and analyse models of structures at the atomic scale, as well as build and represent molecular structures with enhanced graphics. The crystallographic data for anatase presented in Table 1 (Naicker et al., 2005; Jagtap et al., 2005), were used to build an atomistic model of a perfect crystal lattice. Then, using the bulk lattice, atomic Cartesian-coordinates for cylindrical arrays of atoms, representing nanowires of anatase, were calculated for cross-sectional diameters ranging from 2 to 6 nm. In this procedure, the unique crystallographic axis (c axis) of the tetragonal unit cell of anatase was aligned parallel to the unique axis of the cylinder. The origin of the cylindrical coordinate-system, used to describe the nano-wire, was taken to coincide with the origin of the unit cell. A polygonal approximation to a circular boundary condition was made so as to accommodate the discrete positions of atoms with orientations described by Miller indices. The boundary was imposed with the constraint of maintaining charge neutrality overall. Hence, excess surface atoms of titanium and oxygen were removed (Fig. 1) to ensure stoichiometric and electrical neutrality (Okeke et al., 2013) of the wires.

**Table 1** Experimental unit cell parameters and space group for anatase (Horn et al., 1972; Naicker et al., 2005)

The typical average length (L):diameter (D) ratio of nanowires used in previous experiments range between about 10:1 and 20:1 (Shirale et al., 2010; Moshofsky and Mokari, 2013; Gudiksen et al., 2001), however here, this ratio is limited to 6:1 due to computational restrictions on the total number of atoms. The information obtained from the current simulations is useful and indicative of the nano scale properties of TiO<sub>2</sub> in different shapes (Okeke et al., 2016).

**Fig. 1** A typical 3 nm anatase nanowire created using Materials Studio. Ti and O atoms are represented in red and blue colours respectively

The sizes of the particles and their corresponding number of Ti and O atoms are presented in Table 2.

**Table 2** Size nanowires with corresponding number of atoms

## 2.2 Representation of the interatomic potentials

The Matsui – Akaogi force field (Koparde and Cummings, 2005; Filyukov et al., 2007; Koparde and Cummings, 2007; Matsui and Akaogi, 1991) which is widely reported in literature for modelling TiO<sub>2</sub> polymorphs, was used to carry out molecular dynamics simulations in this work. This force field is known to be the most suitable for carrying out atomistic simulations of bulk titania polymorphs for a wide range of temperatures. It is reliable over a range of TiO<sub>2</sub> configurations and is capable of reproducing structures of titania polymorphs which were experimentally determined, and their order of relative stability (Koparde and Cummings, 2007) as a function of particle size (assuming a spherical shape). The mathematical form of the two-body, rigid-ion interatomic potential is expressed as follows.

$$U(r_{ij}) = A_{ij} \exp\left(-\frac{r_{ij}}{\rho_{ij}}\right) - \frac{C_{ij}}{r_{ij}^6} + \frac{q_i q_j}{r_{ij}} \quad (1)$$

Here  $U(r_{ij})$  is the pairwise interaction energy,  $r_{ij}$  is the distance between sites  $i$  and  $j$ . A partial charge occurs when the electrons in chemical bonds are unequally distributed due to differences in electronegativity between atoms (Heinz et al., 2004). Hence, an asymmetric distribution of the electrons occurs. A partial charge model was employed to describe the electrostatic interactions of the Ti and O atoms, with magnitudes of +2.196 and -1.098 (Naicker et al., 2005) respectively. The parameters  $A_{ij}$ ,  $\rho_{ij}$  and  $C_{ij}$ , are provided in Table 3.

**Table 3** Potential parameters for TiO<sub>2</sub> (Oliver et al., 1997)

### **2.2.1 Simulation methodology**

The classical molecular dynamics code, DL\_POLY Version 2 (Smith et al., 2010; Smith and Forester, 1996), was used in this work to carry out molecular dynamics simulations. Newton's equations of motion were integrated using the Verlet leapfrog algorithm within DL\_POLY. Simulations were carried out in the canonical ensemble (NVT), and the temperature of the system was maintained using the Berendsen thermostat (Smith et al., 2010; Berendsen et al., 1984). No periodic boundary conditions were used here. The distance cut-offs for the energy and force calculations were chosen to be greater than the length of the nanowires by 10 Å, to ensure that all atom-atom interactions were taken into account during simulations. The direct Coulomb summation technique available in DL\_POLY was used in calculating the electrostatic interactions. Simulations were carried out for a period of 1 ns, sufficiently long to achieve a steady state in the atomic structure of the particles (Okeke et al., 2016). A time step of 1 fs was used in the simulations.

## **3 Results and discussion**

### **3.1 Thermodynamic properties**

Potential energy variation with temperature for nanowires with cross-sectional diameters between 2 to 6 nm is presented in Fig. 2. A general increase in potential energy with temperature can be observed for rods of all diameters as expected. The melting point of the TiO<sub>2</sub> nano-rods can be estimated from the change in slope of the temperature dependence of the potential energy manifested in the total energy profiles. Melting points and phase transition temperatures have been estimated previously for anatase spherical nanoparticles from total energy profiles (Okeke et al., 2016), where the melting transition temperature was observed to range between 1500 and 2000 K for nanoparticles diameters in the range 3 to 4 nm, and 2000 and 2500 K for diameters in the range 5 to 6 nm. Similar approaches have been employed by

others (Filyukov et al., 2007) who estimated the melting point for anatase nanospheres as 2250 K. In Fig. 2, the rate of change of potential energy (or energy gradient) with temperature is observed to increase linearly especially below the melting-transition temperature for all particle cross-sectional diameters. The melting transition temperature is represented by the region of temperature associated with a pronounced increase in the rate of change of potential energy with temperature. The region of temperature that encompasses this transition is characterised by a temperature range with lower and upper bounds. The gradient of the curve above the melting transition is less than the gradient of the curve below the melting transition reflecting a decrease in the heat capacity at constant volume of the liquid state compared to the solid state. The melting transition temperatures for 3 nm is seen to occur between 1500 and 2000 K, and for 4 to 6 nm, between 2000 and 2500 K. Overall, it can be seen that the melting transition temperature estimated in the current work for nanowires is comparable with those observed in the work of Okeke, et al. (Okeke et al., 2016) and Filyukov et al, (Filyukov et al., 2007) for spherical nanoparticles.

**Fig. 2** Potential energy of 2 – 6 nm size nanowires as a function of temperature

### **3.2 Structural properties**

Radial distribution functions (RDFs) of Ti and O pairs for nanowires of various diameter are shown in Fig. 3 and 4. RDFs describe the variation of atomic number-density as a function of the distance from a reference atom. They can be employed to characterise the structure of liquid and solid phases (Brostow, 1977). RDFs describe the local coordination around a specific atom and represent the internal structure of a material. The probability of locating an atom at a distance  $r$  from a reference atom compared to a homogenous material such as an ideal gas, of the same number density, is represented by the function,  $G(r)$  (Okeke et al., 2016).

This function is useful in estimating the coordination number  $n_{ij}(r)$  for distinct atomic-sites in a structure (Brostow, 1977). In structural analysis, the number of nearest neighbours surrounding a reference/central atom is its coordination number which is also associated with the bond length between the central atom and its neighbouring atoms. The coordination number,  $n_{ij}(r)$ , is given by the following expression (Brostow, 1977);

$$n_{ij}(r) = 4\pi\rho \int_{r_{min}}^{r_{max}} r^2 G(r) dr \quad (2)$$

Where  $\rho$  is the number density and is given as;  $\rho = N/V$  in which case  $N$  is the number of atoms/molecules in a system of volume  $V$ . In this work, coordination numbers of Ti atoms were determined by setting a cut off of 2.3 Å which represents the position of the first minimum after the first peak on the RDF plot (Hines et al., 1985). The coordination numbers of Ti for the different rod diameters and temperatures are reported in Table 4.

**Table 4** Coordination number for corresponding particle size, initial bond length (before simulation), and temperature for anatase TiO<sub>2</sub> nanowires

A bond length of 1.91 Å for all diameters (fixed aspect ratio), can be observed from Table 4, which is similar to bond lengths observed in the literature (Naicker et al., 2005; Okeke et al., 2016; Tang et al., 1993; Zhang et al., 2008; Banfield et al., 1993), but, in those instances, for TiO<sub>2</sub> spherical nanoparticles. A coordination number of 5 for 2 to 6 nm nanowires at temperatures ranging from 300 to 1500 K, can be observed in Table 4. Similarly, for temperatures from 2500 to 3000 K, the nanowires are seen to have a coordination number of 4. In the temperature range from 300 to 1500 K the atoms have relatively highly ordered structures with, typically, highly coordinated atoms. However, as the temperature increases to between 2000 and 3000 K, this is accompanied by an under-coordination of the atoms. The melting point estimated from the total energy profile is seen to fall within the transition temperature region between 2000 and 2500 K in Table 4, where the coordination number drops

from 5 to 4. In Table 4, the system is seen to become tetrahedrally coordinated (i.e. 4-coordinated  $\text{TiO}_n$  units,  $n < 6$ ) as the temperature increases and approaches the transition temperature region, and the coordination number increases with increasing wire diameter (for a constant aspect ratio). The tetrahedral coordination is known to represent liquid or molten systems (Hoang, 2008), and is usually at temperatures of about 3000 K.

Structural configurations in the form of RDFs (generated from the time-averaged RDF values over the entire simulation) for typical cases of 3 and 6 nm diameter nanowires, are shown in Fig. 3 and 4. The trends of the results were identical for other particle sizes, and hence, were not repeated here. The RDFs are observed to transform from a well-ordered to molten configuration for increasing temperature, as also represented in Table 4. The well-ordered configuration is characterised by a profile with predominantly narrow peaks (for temperatures below 2000 K). The molten configuration is characterised by a profile with fewer and broader/stretched-out peaks (for temperatures above 2000 K). The narrow and broad peaks in the profiles of both configurations, can be best observed in the case of 6 nm in Fig. 4. The greater order observed for low temperatures such as 300 K can be attributed to the higher coordination number of nano-rods that are highly crystalline. However, these peaks are seen to broaden and stretch out as the temperature increases. The degree of order of the peaks is seen to decrease with an increase in temperature, and the intensity is seen to reduce for high temperatures of 3000 K. This is the region where the structure is in the liquid state. The temperature at which the peaks start to broaden (i.e. 2000 K) represent the melting transition temperature, similar to what was observed for the melting point estimated from the total energy profile. Overall, an increase in particle diameter from 3 to 6 nm is characterised by an increase in coordinated  $\text{TiO}_2$  units represented by an increase in well-ordered sharp peaks as the particle size increases.

**Fig. 3** RDF's for Ti – Ti, Ti – O and O – O pairs of 3 nm nanowires

**Fig. 4** RDF's for Ti – Ti, Ti – O and O – O pairs of 6 nm nanowires

Structural changes in anatase nanowires after performing molecular dynamics simulations at temperatures between 300 and 3000 K, are shown in Fig. 5. A distortion in the form of bending of the particles is seen to occur at high temperatures, mostly above 2000 K. This is seen to be more obvious in the case of 2 nm, however, the observed bending is seen to decrease as the wire diameter increases, above 4 nm. This trend can be linked to observations made in the variation of potential energy with temperature on the total energy profile, and the RDFs. The melting transition temperature can be associated with the temperature at which the structural bending is seen to occur, which is above 2000 K. Also, the coordination numbers shown in Table 4 are lower for 2 nm, and increases as the wire diameter increases. The structural change of the nanowires presented in Fig. 5, shows a less coordinated structure for 2 nm particle size, however, the coordination is seen to increase as the particle size increases.

**Fig. 5** Structural change of anatase nanowires before and after MD simulation at different temperatures (Ti and O atoms are shown in red and blue colours respectively).

### **3.3 Prediction of inter-wire interaction forces**

Molecular dynamics simulations have been used to predict interaction forces in relation to separation distance between nanowires (Fig.6) with three different orientations (Fig.7) at ambient temperature (300 K). The interaction between similar or dissimilar particles is important in unit operations such as fluidization (Salameh et al., 2012; Larson et al., 1993), coating (Jono et al., 2000), and agglomeration. For small particles (< 10 nm), the effects of molecular structure of the particles (in both vacuum and liquid environments) or the distribution of terminal groups on the surface of the particles (especially in liquid environments), may influence these interactions (Salameh et al., 2012; Ramirez-Garcia et al., 2011). Inter-particle/atomic forces for micro and nanoparticles are usually obtained using

experimental force spectroscopy measurements, for example, using an Atomic Force Microscope (AFM) (Binnig et al., 1986). The observed interaction forces are presented in the form of force-displacement curves as seen in Fig. 8. Force-displacement curves describe the non-contact, attractive and repulsive regions along a separation distance between two materials. These regions represent non-bonded interactions and are independent of an explicit bonding connection between materials. The interaction plot (Fig. 6) depicts a region in which a long-range attractive force (i.e. van der Waals force) is experienced, and a region at smaller separation distances in which a short-range repulsive force (i.e. Lennard-Jones, Morse force etc.) is experienced. Modelling of these interactions is dependent on the distance between the particles and so these through-space interactions are usually modelled as a function of an inverse power of the distance (Leach, 2001). In force fields, the non-bonded terms are usually regarded as electrostatic interactions and van der Waals interactions (or dispersion forces).

**Fig. 6** A typical force-displacement curve showing the non-contact, attractive and repulsive regimes

Force-displacement curves for separation distances between two nanowires at different orientations have been obtained using a molecular dynamics simulation approach, within the DL\_POLY package. The orientations are shown in 2D in Fig. 7. The approach used involved fixing a formula unit of  $\text{TiO}_2$  in each particle at the centre of mass of the particles, so that the particles were constrained to their centre of mass separation distances. The particles were constrained to their centre of mass distance for a series of simulations, and were only advanced towards each other, prior to each simulation. Each simulation formed a separation distance, and the interparticle force was averaged over each simulation. The separation distance and calculated interparticle forces obtained from the series of simulations, were used to produce a force-displacement curve.

**Fig. 7** 2D orientations of nanowires for interaction force predictions (a) parallel, (b) perpendicular, and (c) end-to-end. Ti and O atoms are shown in red and blue colours respectively.

The separation distance used in the Fig. 8 was the surface-to-surface distance between two nanowires of different orientations (Fig.7). There is limited information with regards to studies on interaction forces between nanowires in the literature, however, the magnitude of the forces in our study are in good agreement with those for spherical nanoparticles available in the literature (Laube, et al 2015). In the current study, the particles were initially separated at a distance of 20 nm, and they started to attract to each other at a separation distance of about 8 nm for the end-to-end orientation, and 6 nm for both parallel and perpendicular orientations. In all three cases of orientations, the particles are seen to be most attractive at a separation distance of 4 nm, after which, they become repulsive. Also, the end-to-end orientation is seen to possess the most attractive (strongest attraction) and repulsive forces, while the parallel and perpendicular orientations are seen to possess the lower attractive (weaker attraction) and repulsive forces. This can be observed from the magnitude of their forces, where the end-to-end orientation is seen to have attractive and repulsive forces of -0.38 and 0.15 nN, respectively, whereas, the parallel and perpendicular orientations are seen to have attractive and repulsive forces of -0.1 and an average of 0.01 nN, respectively. The stronger attraction observed in the case of end-to-end orientations can be attributed to the high surface area (diameter-wise) of the two interacting surfaces in contact. However, the parallel orientation had both contact surfaces (length-wise) with low surface area. The perpendicular orientation had one surface with high surface area (diameter-wise), and low contact surface area (length-wise), hence the weaker attraction observed. It is also recognised that high surface area to volume ratio of nanoparticles is relatively more favourable to interparticle interactions than for particles of macroscopic size.

**Fig. 8** Force-displacement curve for 2 nm nanowire showing different orientations

## 4 Conclusion

Molecular dynamics simulations have been carried out to investigate the thermodynamic and structural properties, as well as interaction forces of anatase TiO<sub>2</sub> nanowires. Melting points of the nanowires of different cross-sectional diameters, were estimated from the variation of potential energy of the system with temperature from the total energy profile. It was observed that the temperature associated with the melting transition increased with increasing particle size. The melting transition temperature was estimated to be between 2000 and 2500 K, and was similar to that for spherical TiO<sub>2</sub> nanoparticles studied previously. This suggests that the melting point of TiO<sub>2</sub> nanoparticles is independent of the shape of the particles for the size range considered in this work. The RDFs were characterised with peaks which were highly ordered at low temperatures, and broadened out at high temperatures. This trend was linked to the variation of potential energy of the system, and hence, to the melting transition temperature. The melting transition temperature occurred at similar temperatures associated with the broadening of peaks in the RDFs. Furthermore, interaction forces of the particles have been predicted for different orientations. The end-to-end orientation was observed to possess stronger attraction force, and attributed to the high surface area (diameter-wise) of the two surfaces in contact. However, both parallel and perpendicular orientations had contact surfaces with relatively low surface area (length-wise), hence resulting in weaker attraction forces.

These results increase our fundamental understanding of the structural and thermal properties of titania nanowires which could assist in future research in key areas such as developing enhanced heat transfer fluids for energy generation and storage, as well as enhanced drug targeting and delivery for which information on the interaction between individual wires would

be crucial in evaluating their macro-scale properties. Further studies are required to evaluate the interaction forces between nanowires under a wide range of conditions including varying temperature, aspect ratio and for other shapes. Further understanding is required on the variation of interaction forces in relation to the location of the contact point of the contiguous nano wires on their surfaces. Also, future studies are desired to extend the current simulations under a longer time duration than the present cases by using more computing resources.

**Conflict of Interest:** The authors declare that they have no conflict of interest

## References

- Abdullah, H.Kuo, D.-H.Kuo, Y.-R.Yu, F.-A. and Cheng, K.-B. 2016. Facile Synthesis and Recyclability of Thin Nylon Film-Supported n-Type ZnO/p-Type Ag<sub>2</sub>O Nano Composite for Visible Light Photocatalytic Degradation of Organic Dye. *The Journal of Physical Chemistry C*. **120**(13), pp.7144-7154.
- Acharya, S. and Efrima, S. 2005. Two-Dimensional Pressure-Driven Nanorod-to-Nanowire Reactions in Langmuir Monolayers at Room Temperature. *Journal of the American Chemical Society*. **127**(10), pp.3486-3490.
- Banfield, J.F.Bischoff, B.L. and Anderson, M.A. 1993. TiO<sub>2</sub> accessory minerals: coarsening, and transformation kinetics in pure and doped synthetic nanocrystalline materials. *Chemical Geology*. **110**(1-3), pp.211-231.
- Berendsen, H.J.C.Postma, J.P.M.van Gunsteren, W.F.DiNola, A. and Haak, J.R. 1984. Molecular dynamics with coupling to an external bath. *The Journal of Chemical Physics*. **81**(8), pp.3684-3690.
- Binnig, G.Quate, C.F. and Gerber, C. 1986. Atomic Force Microscope. *Physical Review Letters*. **56**(9), pp.930-933.
- Boal, A.K.Ilhan, F.DeRouchey, J.E.Thurn-Albrecht, T.Russell, T.P. and Rotello, V.M. 2000. Self-assembly of nanoparticles into structured spherical and network aggregates. *Nature*. **404**(6779), pp.746-748.
- Brostow, W. 1977. Radial distribution function peaks and coordination numbers in liquids and in amorphous solids. *Chemical Physics Letters*. **49**(2), pp.285-288.
- Chaudhari, G.N.Bambole, D.R.Bodade, A.B. and Padole, P.R. 2006. Characterization of nanosized TiO<sub>2</sub> based H<sub>2</sub>S gas sensor. *Journal of Materials Science*. **41**(15), pp.4860-4864.
- Chen, X. and Mao, S.S. 2006. Synthesis of titanium dioxide (TiO<sub>2</sub>) nanomaterials. *J Nanosci Nanotechnol*. **6**(4), pp.906-25.

- De Jong, W.H. and Borm, P.J.A. 2008. Drug delivery and nanoparticles: Applications and hazards. *International Journal of Nanomedicine*. **3**(2), pp.133-149.
- Ding, Y.Chen, H.Musina, Z.Jin, Y.Zhang, T.Witharana, S. and Yang, W. 2010. Relationship between the thermal conductivity and shear viscosity of nanofluids. *Physica Scripta*. **T139** (2010).
- Dong, K.J.Yang, R.Y.Zou, R.P. and Yu, A.B. 2006. Role of Interparticle Forces in the Formation of Random Loose Packing. *Physical Review Letters*. **96**(14), p145505.
- Duncan, R. 2003. The dawning era of polymer therapeutics. *Nat Rev Drug Discov*. **2**(5), pp.347-360.
- Ferrari, M. 2005. Cancer nanotechnology: opportunities and challenges. *Nat Rev Cancer*. **5**(3), pp.161-171.
- Filyukov, D.Brodskaya, E.Piotrovskaya, E. and de Leeuw, S. 2007. Molecular-dynamics simulation of nanoclusters of crystal modifications of titanium dioxide. *Russian Journal of General Chemistry*. **77**(1), pp.10-16.
- Francioso, L.Taurino, A.M.Forleo, A. and Siciliano, P. 2008. TiO<sub>2</sub> nanowires array fabrication and gas sensing properties. *Sensors and Actuators B: Chemical*. **130**(1), pp.70-76.
- Garg, P.Alvarado, J.L.Marsh, C.Carlson, T.A.Kessler, D.A. and Annamalai, K. 2009. An experimental study on the effect of ultrasonication on viscosity and heat transfer performance of multi-wall carbon nanotube-based aqueous nanofluids. *International Journal of Heat and Mass Transfer*. **52**(21-22), pp.5090-5101.
- Gorkhover, T.Schorb, S.Coffee, R.Adolph, M.Foucar, L.Rupp, D.Aquila, A.Bozek, J.D.Epp, S.W.Erk, B.Gumprecht, L.Holmegaard, L.Hartmann, A.Hartmann, R.Hauser, G.Holl, P.Hömke, A.Johnsson, P.Kimmel, N.Kühnel, K.-U.Messerschmidt, M.Reich, C.Rouzée, A.Rudek, B.Schmidt, C.Schulz, J.Soltau, H.Stern, S.Weidenspointner, G.White, B.Küpper, J.Strüder, L.Schlichting, I.Ullrich, J.Rolles, D.Rudenko, A.Möller, T. and Bostedt, C. 2016. Femtosecond and nanometre visualization of structural dynamics in superheated nanoparticles. *Nat Photon*. **10**(2), pp.93-97.
- Gudiksen, M.S.Wang, J. and Lieber, C.M. 2001. Synthetic Control of the Diameter and Length of Single Crystal Semiconductor Nanowires. *The Journal of Physical Chemistry B*. **105**(19), pp.4062-4064.
- Haverkamp, R.G. 2010. A Decade of Nanoparticle Research in Australia and New Zealand. *Particulate Science and Technology: An International Journal*. **28**(1), pp.1 - 40.
- Heinz, H., and Suter, U. 2004. Atomic charges for classical simulations of polar systems. *Journal of Physical Chemistry B* **108**(47), pp 18341-18352
- Hines, A.Walls, H. and Jethani, K. 1985. Determination of the coordination number of liquid metals near the melting point. *Metallurgical Transactions A*. **16**(1), pp.267-274.
- Hoang, V.V. 2008. The glass transition and thermodynamics of liquid and amorphous TiO<sub>2</sub> nanoparticles. *Nanotechnology*. **19**(10), p105706.

- Horn, M.Schwerdtfeger, C. and Meagher, E. 1972. Refinement of the structure of anatase at several temperatures. *Zeitschrift für Kristallographie*. **136**(3-4), p273.
- Hwang, Y.J.Hahn, C.Liu, B. and Yang, P. 2012. Photoelectrochemical Properties of TiO<sub>2</sub> Nanowire Arrays: A Study of the Dependence on Length and Atomic Layer Deposition Coating. *ACS Nano*. **6**(6), pp.5060-5069.
- Jagtap, N.Bhagwat, M.Awati, P. and Ramaswamy, V. 2005. Characterization of nanocrystalline anatase titania: an in situ HTXRD study. *Thermochimica Acta*. **427**(1-2), pp.37-41.
- Jono, K.Ichikawa, H.Miyamoto, M. and Fukumori, Y. 2000. A review of particulate design for pharmaceutical powders and their production by spouted bed coating. *Powder Technology*. **113**(3), pp.269-277.
- Karmakar, S.Kumar, S.Rinaldi, R. and Maruccio, G. 2011. Nano-electronics and spintronics with nanoparticles. *Journal of Physics: Conference Series*. **292**(1), p012002.
- Koparde, V.N. and Cummings, P.T. 2005. Molecular Dynamics Simulation of Titanium Dioxide Nanoparticle Sintering. *The Journal of Physical Chemistry B*. **109**(51), pp.24280-24287.
- Koparde, V.N. and Cummings, P.T. 2007. Molecular Dynamics Study of Water Adsorption on TiO<sub>2</sub> Nanoparticles. *The Journal of Physical Chemistry C*. **111**(19), pp.6920-6926.
- Kulkarni, A.Rao, P.Natarajan, S.Goldman, A.Sabbiseti, V.S.Khater, Y.Korimerla, N.Chandrasekar, V.Mashelkar, R.A. and Sengupta, S. 2016. Reporter nanoparticle that monitors its anticancer efficacy in real time. *Proceedings of the National Academy of Sciences*. **113**(15), pp.E2104-E2113.
- Larson, I.Drummond, C.J.Chan, D.Y.C. and Grieser, F. 1993. Direct force measurements between titanium dioxide surfaces. *Journal of the American Chemical Society*. **115**(25), pp.11885-11890.
- Leach, A. 2001. *Molecular Modelling: Principles and Applications (2nd Edition)*. Prentice Hall.
- Lin, H.Li, L.Zhao, M.Huang, X.Chen, X.Li, G. and Yu, R. 2012. Synthesis of High-Quality Brookite TiO<sub>2</sub> Single-Crystalline Nanosheets with Specific Facets Exposed: Tuning Catalysts from Inert to Highly Reactive. *Journal of the American Chemical Society*. **134**(20), pp.8328-8331.
- Mahshid, S.Askari, M. and Ghamsari, M.S. 2007. Synthesis of TiO<sub>2</sub> nanoparticles by hydrolysis and peptization of titanium isopropoxide solution. *Journal of Materials Processing Technology*. **189**(1-3), pp.296-300.
- Materials Studio suite of crystallographic programs*. [Online]. Available from: <http://accelrys.com/products/collaborative-science/biovia-materials-studio/>.
- Matsui, M. and Akaogi, M. 1991. Molecular Dynamics Simulation of the Structural and Physical Properties of the Four Polymorphs of TiO<sub>2</sub>. *Molecular Simulation*. **6**(4-6), pp.239-244.

- Min, Y. Akbulut, M. Kristiansen, K. Golan, Y. and Israelachvili, J. 2008. The role of interparticle and external forces in nanoparticle assembly. *Nat Mater.* **7**(7), pp.527-538.
- Mohd Azlishah, O. Noor Faridah, A. Badrul Hisham, A. and Jose, R. 2014. Electrical Conductivity Characteristic of TiO<sub>2</sub> Nanowires From Hydrothermal Method. *Journal of Physics: Conference Series.* **495**(1), p012027.
- Moshofsky, B. and Mokari, T. 2013. Length and Diameter Control of Ultrathin Nanowires of Substoichiometric Tungsten Oxide with Insights into the Growth Mechanism. *Chemistry of Materials.* **25**(8), pp.1384-1391.
- Naicker, P.K. Cummings, P.T. Zhang, H. and Banfield, J.F. 2005. Characterization of Titanium Dioxide Nanoparticles Using Molecular Dynamics Simulations. *The Journal of Physical Chemistry B.* **109**(32), pp.15243-15249.
- Okeke, G. Hammond, R.B. and Antony, S.J. 2013. Molecular Dynamics Simulation of Anatase TiO<sub>2</sub> Nanoparticles. *Journal of Nanoscience and Nanotechnology.* **13**(2), pp.1047-1052.
- Okeke, G. Hammond, R.B. and Antony, S.J. 2016. Effects of heat treatment on the atomic structure and surface energy of rutile and anatase TiO<sub>2</sub> nanoparticles under vacuum and water environments. *Chemical Engineering Science.* **146**, pp.144-158.
- Okeke, G. Witharana, S. Antony, S. and Ding, Y. 2011. Computational analysis of factors influencing thermal conductivity of nanofluids. *Journal of Nanoparticle Research.* **13**(12), pp.6365-6375.
- Oliver, P.M. Watson, G.W. Toby Kelsey, E. and Parker, S.C. 1997. Atomistic simulation of the surface structure of the TiO<sub>2</sub> polymorphs rutile and anatase. *Journal of Materials Chemistry.* **7**(3), pp.563-568.
- Pradhan, N. and Efrima, S. 2004. Supercrystals of Uniform Nanorods and Nanowires, and the Nanorod-to-Nanowire Oriented Transition. *The Journal of Physical Chemistry B.* **108**(32), pp.11964-11970.
- Pritesh, H. Husnu Emrah, U. and Gehan, A.J.A. 2012. Nanowires for energy generation. *Nanotechnology.* **23**(19), p194002.
- Ramirez-Garcia, S. Chen, L. Morris, M.A. and Dawson, K.A. 2011. A new methodology for studying nanoparticle interactions in biological systems: dispersing titania in biocompatible media using chemical stabilisers. *Nanoscale.* **3**(11), pp.4617-24.
- Salameh, S. Schneider, J. Laube, J. Alessandrini, A. Facci, P. Seo, J.W. Ciacchi, L.C. and Mädler, L. 2012. Adhesion Mechanisms of the Contact Interface of TiO<sub>2</sub> Nanoparticles in Films and Aggregates. *Langmuir.* **28**(31), pp.11457-11464.
- Shirale, D.J. Bangar, M.A. Chen, W. Myung, N.V. and Mulchandani, A. 2010. Effect of Aspect Ratio (Length:Diameter) on a Single Polypyrrole Nanowire FET Device. *The Journal of Physical Chemistry C.* **114**(31), pp.13375-13380.
- Smith, W. and Forester, T.R. 1996. DL\_POLY\_2.0: A general-purpose parallel molecular dynamics simulation package. *Journal of Molecular Graphics.* **14**(3), pp.136-141.

- Smith, W.Forester, T.R. and Todorov, I.T. 2010. The DL\_POLY\_2 User Manual. *STFC Daresbury Laboratory*. **Version 2.21**.
- Soo-Jin Park, Y.C.K., Ju Y. Park, Ed A. Evans, Rex D. Ramsier, and George G. Chase. 2010. Physical Characteristics of Titania Nanofibers Synthesized by Sol-Gel and Electrospinning Techniques. *Journal of Engineered Fibers and Fabrics*. **5(1)**, pp.50-56.
- Tang, H.Berger, H.Schmid, P.E.Lévy, F. and Burri, G. 1993. Photoluminescence in TiO<sub>2</sub> anatase single crystals. *Solid State Communications*. **87(9)**, pp.847-850.
- Xu, Z.P.Zeng, Q.H.Lu, G.Q. and Yu, A.B. 2006. Inorganic nanoparticles as carriers for efficient cellular delivery. *Chemical Engineering Science*. **61(3)**, pp.1027-1040.
- Zeng, Q.Yu, A. and Lu, G. 2010. Evaluation of Interaction Forces between Nanoparticles by Molecular Dynamics Simulation. *Industrial & Engineering Chemistry Research*. **49(24)**, pp.12793-12797.
- Zhang, H.Chen, B.Banfield, J.F. and Waychunas, G.A. 2008. Atomic structure of nanometer-sized amorphous TiO<sub>2</sub>. *Physical Review B*. **78(21)**, p214106.
- Zheng, L.Xu, M. and Xu, T. 2000. TiO<sub>2-x</sub> thin films as oxygen sensor. *Sensors and Actuators B: Chemical*. **66(1-3)**, pp.28-30.

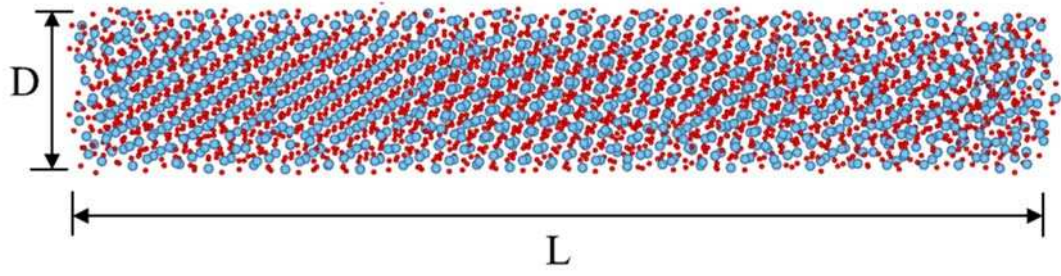


Fig.1 A typical 3 nm anatase nanowire created using Materials Studio. Ti and O atoms are represented in red and blue colours respectively

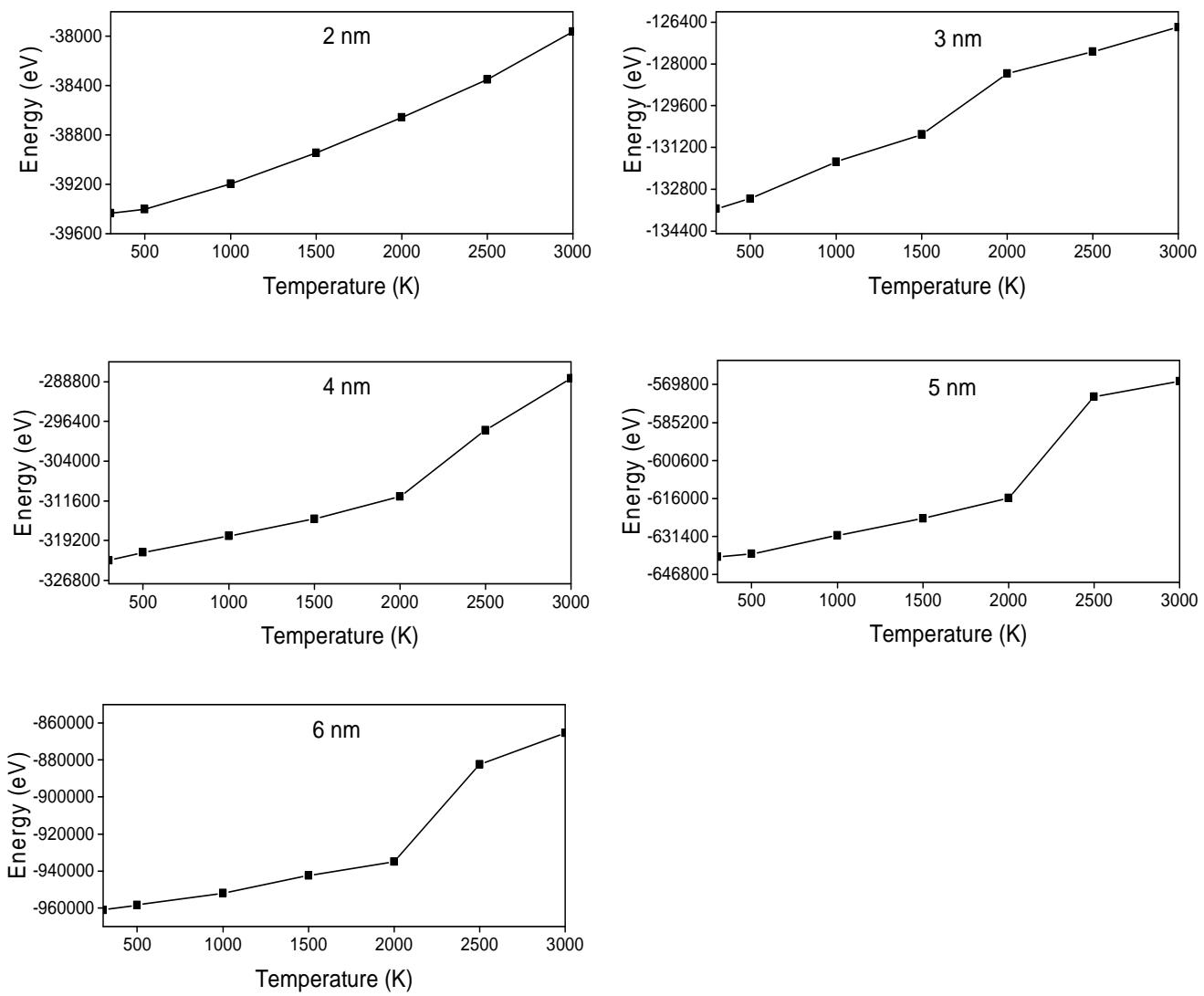


Fig.2 Potential energy of 2 – 6 nm size nanowires as a function of temperature

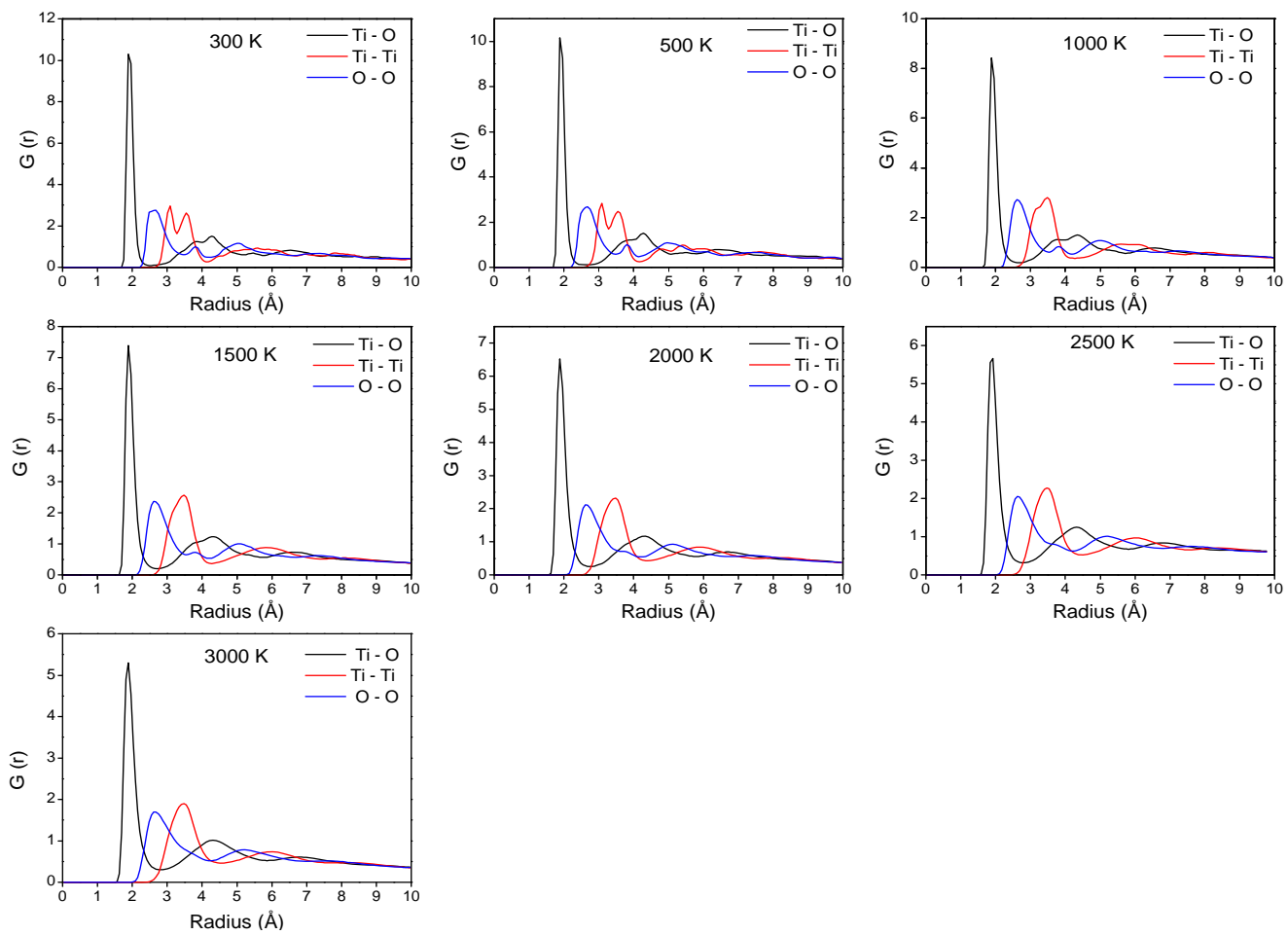


Fig.3 RDF's for Ti – Ti, Ti – O and O – O pairs of 3 nm nanowires

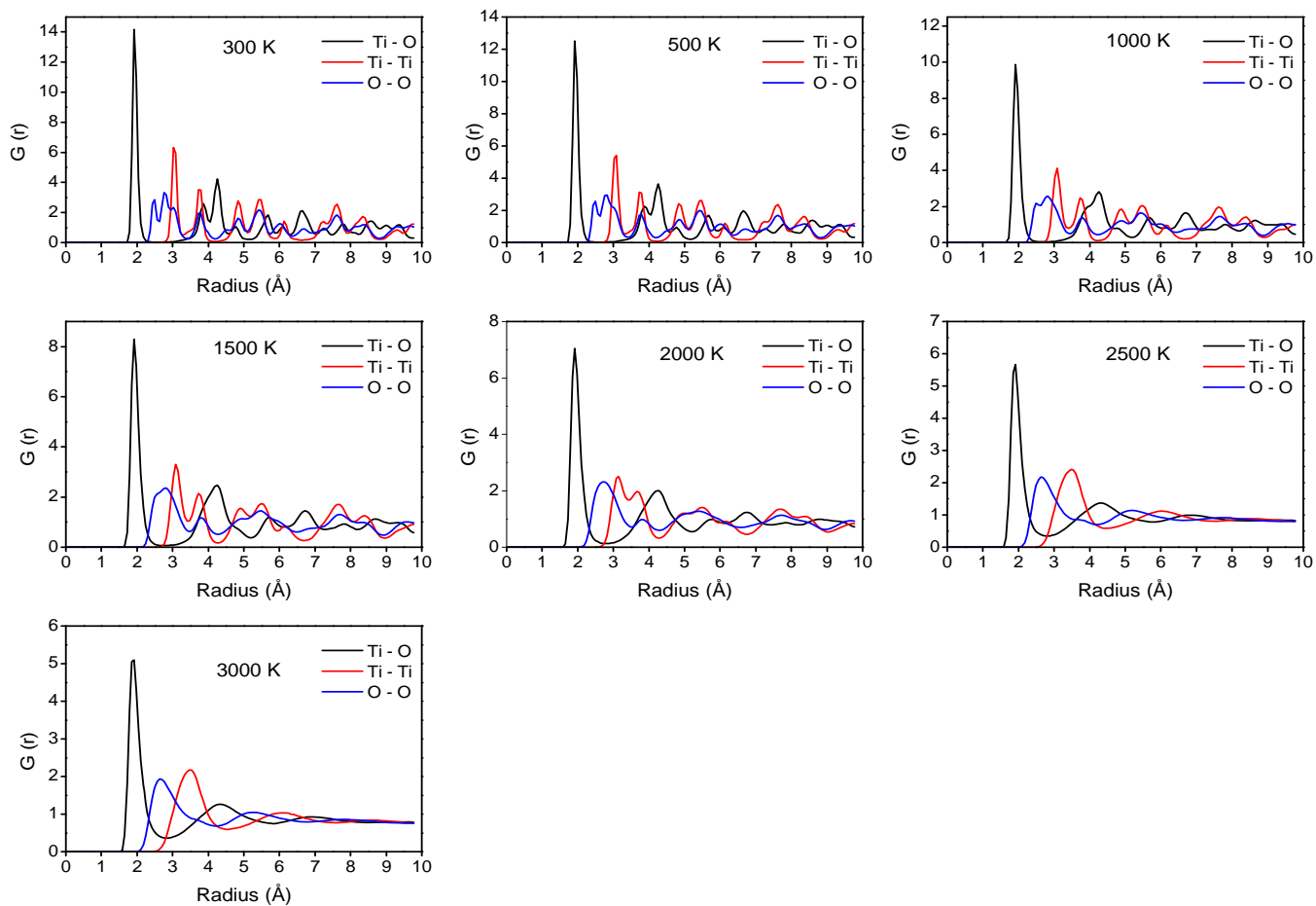


Fig.4 RDF's for Ti – Ti, Ti – O and O – O pairs of 6 nm nanowires

Size (nm)	Before Simulation	Simulations at						
		300 K	500 K	1000 K	1500 K	2000 K	2500 K	3000 K
Nano-wires								
2								
3								
4								
5								

Fig.5 Structural change of anatase nanowires before and after MD simulation at different temperatures (Ti and O atoms are shown in red and blue colours respectively).

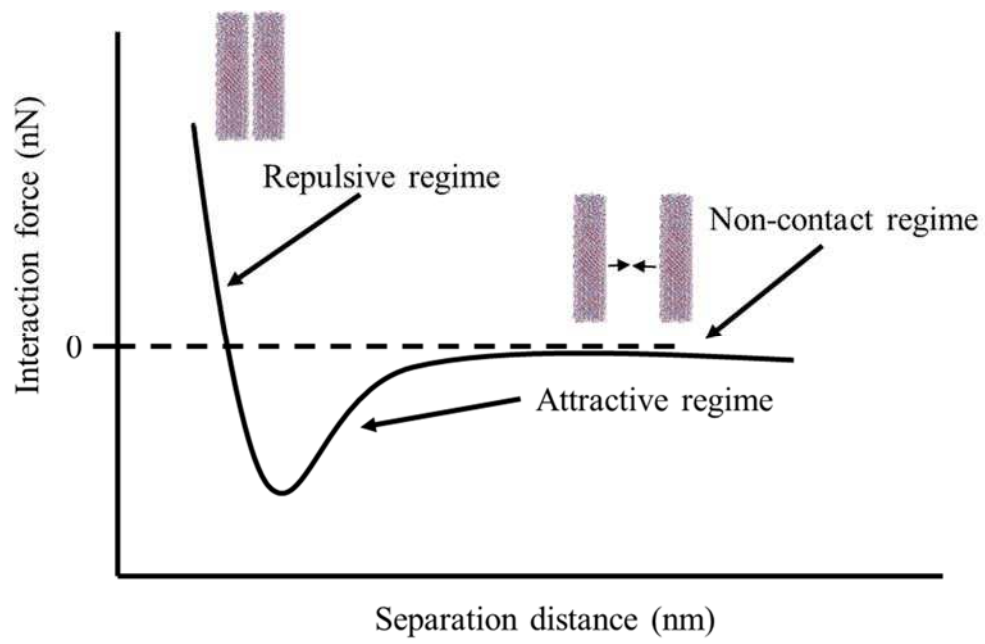


Fig.6 A typical force-displacement curve showing the non-contact, attractive and repulsive regimes

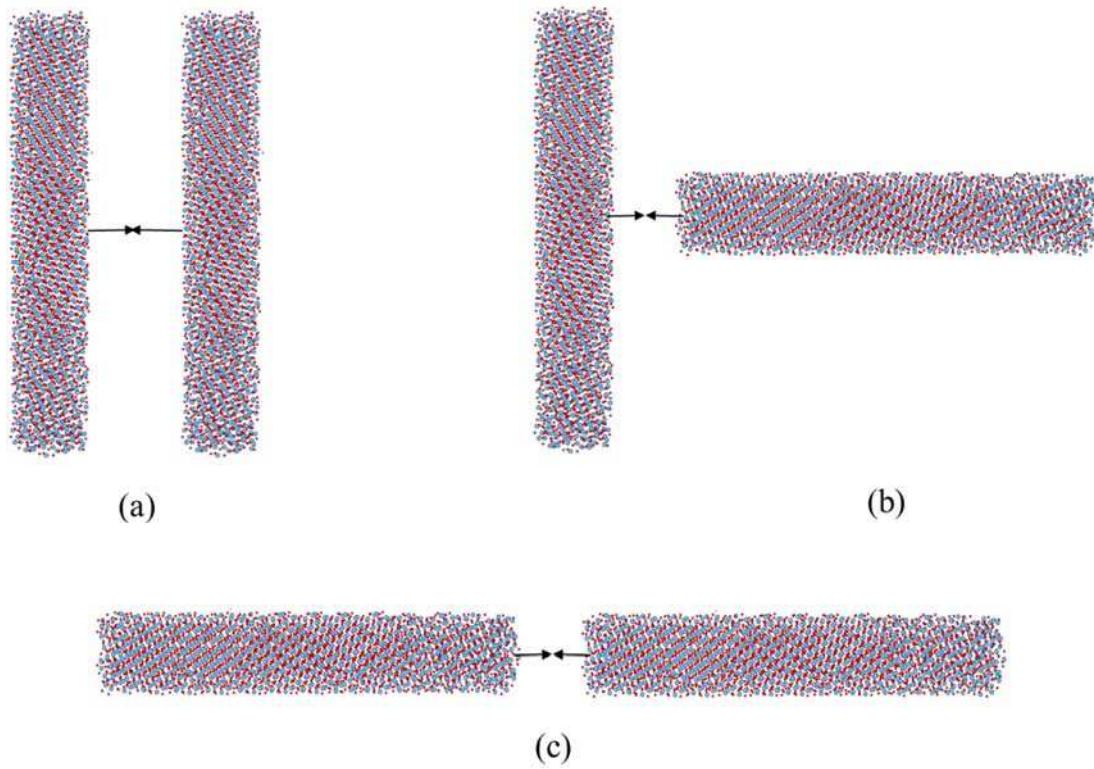


Fig.7 2D view of the orientations of nanowires for studying their interactions (a) parallel, (b) perpendicular, and (c) end-to-end. Ti and O atoms are shown in red and blue colours respectively.

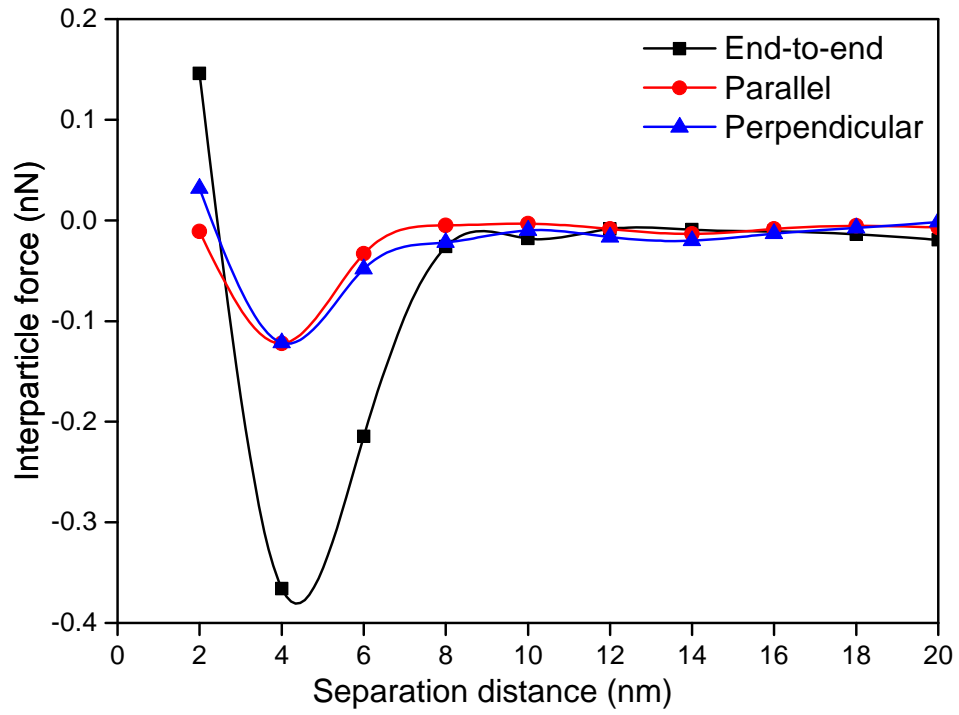


Fig.8 Force-displacement curve for 2 nm nanowire showing different orientations

Table 1 Experimental unit cell parameters and space group for anatase (Horn et al., 1972; Naicker et al., 2005)

<b>Phase</b>	<b>Crystal System</b>	<b>Space group</b>	<b><i>a</i>, Å</b>	<b><i>b</i>, Å</b>	<b><i>c</i>, Å</b>
Anatase	Tetragonal	<i>I41/amd</i>	3.784	3.784	9.514

Table 2 Size of the nanowires with corresponding number of atoms

<b>Diameter (nm)</b>	<b>No. of Ti atoms</b>	<b>No. of O atoms</b>	<b>Total no. of atoms</b>
2	1124	2248	3372
3	3644	7288	10932
4	8812	17624	26436
5	17421	34842	52263
6	30037	60074	90111

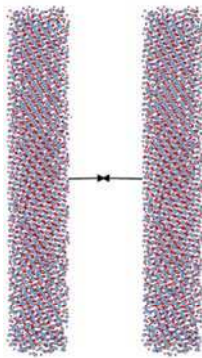
Table 3 Potential parameters for TiO<sub>2</sub> (Oliver et al., 1997)

<b>Interaction</b>	<b><math>A_{ij}/\text{eV}</math></b>	<b><math>\rho_{ij}/\text{\AA}</math></b>	<b><math>C_{ij}/\text{eV \AA}^6</math></b>
Ti - O	16957.53	0.194	12.59
Ti - Ti	31120.2	0.154	5.25
O - O	11782.76	0.234	30.22

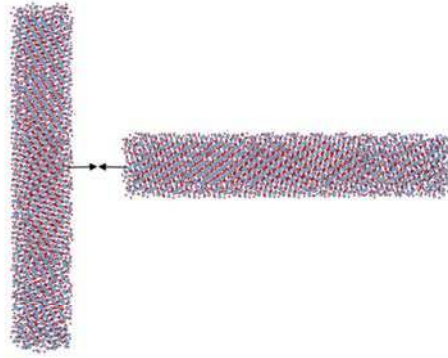
Table 4 Coordination number for corresponding particle size, initial bond length (before simulation), and temperature for anatase TiO<sub>2</sub> nanowires

Wire diameter (nm)	( $\text{\AA}$ )	$(r)$						
		Mostly ordered state				Transition state		Liquid state
		Ti - O	300 K	500 K	1000 K	1500 K	2000 K	2500 K
2	1.91	5.55	5.55	5.41	5.22	4.96	4.71	4.50
3	1.91	5.63	5.62	5.44	5.24	5.01	4.76	4.54
4	1.91	5.74	5.73	5.61	5.31	5.05	4.80	4.60
5	1.91	5.87	5.87	5.62	5.42	5.11	4.88	4.67
6	1.91	5.96	5.95	5.70	5.54	5.23	4.99	4.74

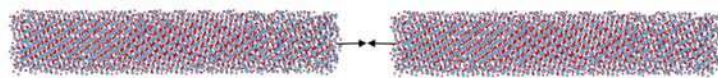
## Graphical abstract



(a)



(b)



(c)